Journal of Electroceramics, 11, 179–189, 2003

Stability and Thermal Expansion of Na^+-Conducting Ceramics

O.A. SMIRNOVA,[1,*,†] R.O. FUENTES,[1,2] F. FIGUEIREDO,[1,3] V.V. KHARTON[1,4] & F.M.B. MARQUES[1]

[1]*Department of Ceramics and Glass Engineering, CICECO, University of Aveiro, 3810-193 Aveiro, Portugal*
[2]*CINSO-CITEFA-CONICET, J.B. de la Salle 4397, B1603ALO Villa Martelli, Buenos Aires, Argentina*
[3]*Science & Technology Department, Universidade Aberta, R. Esc. Politecnica 147, 1269-001 Lisbon, Portugal*
[4]*Institute of Physicochemical Problems, Belarus State University, 14 Leningradskaya Str., 220050 Minsk, Belarus*

Submitted July 23, 2003; Revised December 18, 2003; Accepted January 9, 2004

Abstract. An impedance spectroscopy study of sodium cation-conducting ceramics, including layered compounds $Na_{0.8}Ni_{0.4}Ti_{0.6}O_2$, $Na_{0.8}Fe_{0.8}Ti_{0.2}O_2$, $Na_{0.8}Ni_{0.6}Sb_{0.4}O_2$ (structural type O3), $Na_{0.68}Ni_{0.34}Ti_{0.66}O_2$ (P2 type), and NASICON-type $Na_3Si_2Zr_{1.88}Y_{0.12}PO_{11.94}$ and $Na_{3.2}Si_{2.2}Zr_{1.88}Y_{0.12}P_{0.8}O_{11.94}$, showed that their transport properties are essentially independent of partial water vapor pressure at temperatures above 420 K. In the low-temperature range, increasing vapor partial pressure from approximately 0 (dry air) up to 0.46 atm. leads to a reversible increase in the conductivity. The sensitivity of studied materials to air humidity is strongly affected by the ceramic microstructure, being favored by larger boundary area and porosity. Maximum stability in wet atmospheres was found for NASICON ceramics, which also exhibit the highest cationic conduction. The average thermal expansion coefficients at 300–1173 K are in the range (13.7–16.0) $\times 10^{-6}$ K^{-1} for the layered materials and (5.9–6.5) $\times 10^{-6}$ K^{-1} for NASICON-type ceramics.

Keywords: sodium cationic conductor, impedance spectroscopy, air humidity, thermal expansion, ceramic microstructure

1. Introduction

Solid-state alkali-cation conductors are receiving great attention for applications in rechargeable batteries [1], ion selective electrodes [2, 3], membranes for CO_2-selective and humidity sensors [4–6]. Fast cation transport requires a crystal structure with favorable diffusion pathways, where the metal-oxygen polyhedra occupied by charge carriers should be connected in one (tunnel structures), two (layered structures) or, most preferable, three dimensions forming a pathway through the unit cell. One of the best groups of sodium ion conductors, the so-called NASICONs, is characterized by a lattice with three-dimensional conductivity paths [7]; β-alumina has a layered structure [8]. Another family of layered compounds, having cationic transport properties comparable to those of NASICONs, comprises several structural types based on brucite-like layers $MO_{6/3}$ (where M is transition metal) sandwiching alkali cations [1, 9–14]. The nomenclature developed for these phases [9] separates known structures into P3, O3, P2, O2, O6 and T2, where the letter indicates the coordination of the interlayer alkali cation (**O**ctahedral, trigonal **P**rismatic and **T**etrahedral) and the number shows how many layers compose one unit cell. Such crystal lattices comprise a lot of free space between layers where water can be intercalated to solvate alkali cations [14]. The NASICON-type ceramics are also well known to easily hydrate [15–17]. Potential applications of Na^+ ionic conductors in batteries and fuel cells require maximum stability, including possible minimum reactivity with water. On the other hand, materials showing a significant and reversible response to the humidity variations can be considered for sensor applications.

This work was focused on the comparative study of several layered phases (O3 and P2 types) and

*To whom all correspondence should be addressed. E-mail: osmirnova@cv.ua.pt
†Present address: Department of Ceramics and Glass Engineering, CICECO, University of Aveiro, 3810-193 Aveiro, Portugal.

NASICONs, in order to evaluate their stability in H_2O-containing atmospheres and to assess possible interaction mechanisms with water vapor. To our knowledge, there is no literature data on phase formation in the system Na_2O–NiO–Sb_2O_5. By analogy with titanate systems Na_2O–MO_x–TiO_2 (M = Ni^{2+}, Co^{2+}, Fe^{3+}) [10–13], the authors supposed formation of mixed sodium-nickel antimonates with layered structures; the present work reports characterization of a new Sb-contatining compound in comparison with the isostructural titanates. Another particular goal was to determine thermal expansion of Na^+-conducting ceramics. The values of thermal expansion coefficients (TECs), determining compatibility with other materials at elevated temperatures is of major relevance for device fabrication or integration.

2. Experimental

Dense ceramic samples of $Na_{0.8}Ni_{0.4}Ti_{0.6}O_2$, $Na_{0.8}Fe_{0.8}Ti_{0.2}O_2$, $Na_{0.8}Ni_{0.6}Sb_{0.4}O_2$ (O3-type), $Na_{0.68}Ni_{0.34}Ti_{0.66}O_2$ (P2-type), $Na_3Si_2Zr_{1.88}Y_{0.12}PO_{11.94}$ and $Na_{3.2}Si_{2.2}Zr_{1.88}Y_{0.12}P_{0.8}O_{11.94}$ (NASICON) were prepared by a conventional solid-state reaction technique. For the synthesis of layered compounds, starting materials included $Na_2CO_3{\cdot}10H_2O$ (Merck), $Ni(NO_3)_2{\cdot}6H_2O$ (Aldrich), Fe_2O_3 (Merck), TiO_2 (Merck), and Sb_2O_5 (Aldrich); the NASICON phases were synthesized from $(ZrO_2)_{0.97}(Y_2O_3)_{0.03}$ (TZP, Tosoh), $Na_3PO_4{\cdot}12H_2O$ (Merck), $Na_2CO_3{\cdot}10H_2O$ (Merck) and SiO_2 (Merck). The appropriate amounts of the reagents were ball-milled with ethanol, dried and calcined; this procedure was repeated several times to obtain almost single-phase powders. Then the powders were uniaxially compacted into disks (diameter 1.0–1.8 cm), isostatically pressed at 200 MPa, and sintered in closed platinum crucibles or in packing powder of the same composition in closed alumina containers in order to prevent sodium losses. The sintering conditions and the abbreviations, used below, are listed in Table 1. Note that, as the high temperature processing may be accompanied with sodium losses due to volatilization, the temperature and time of sintering were chosen to the minimum necessary to obtain dense ceramics.

Phase purity of the ceramic materials was verified by X-ray diffraction (XRD) analysis. The spectra were collected using a Rigaku D/Max-B instrument (Cu K_α radiation, graphite monochromator). Crystal structure refinement was performed using the FullProf software [18], Chekcell program was used to calculate unit cell parameters in the case of hydrated phases. Ceramic microstructure was examined by scanning electron microscopy (SEM) using a Hitachi S4100 instrument; the samples for SEM studies were polished and thermally etched for 0.5 h at temperatures 100–200 K lower than the sintering temperature. Thermal expansion was measured by an alumina Linseis dilatometer at 300–1173 K in air (heating rate of 5 K/min). The electrical properties were studied by impedance spectroscopy with a Hewlett Packard 4284A LCR meter in the frequency range from 20 Hz up to 1 MHz. The measurements were performed in a flow of dry air, dry argon and humidified air where the water vapor partial pressure, $p(H_2O)$, varied from approximately 0 up to 0.46 atm. Wetting of the air flow was achieved by bubbling through deionized water at various temperatures (controlled with an accuracy of 1 K). For each measurement, the samples were kept in humidified air flow up to 24 h until the conductivity becomes independent on time. Thermogravimetric and differential thermal analysis (TG/DTA) was

Table 1. Sintering conditions and physicochemical properties of ceramic materials.

Composition	Sintering	ρ_{exp} (g/cm^3)	ρ_{exp}/ρ_{theor}* (%)	Grain size (μm)	σ (mS/cm) 573 K, dry air	E_a (kJ/mol) dry air	$\sigma_{wet}\sigma_{dry}$** 373 K	TEC $\alpha \times 10^6$, K^{-1} 300–1173 K
$Na_{0.68}Ni_{0.34}Ti_{0.66}O_2$	1373 K, 3 h	3.65	94	8.0	97.0	32	1.20	15.70 ± 0.06
$Na_{0.8}Ni_{0.4}Ti_{0.6}O_2$	1298 K, 3 h	3.69	91	3.8	10.9	37	1.16	14.79 ± 0.09
$Na_{0.8}Ni_{0.6}Sb_{0.4}O_2$	1543 K, 3 h	4.62	91	2.7	3.20	48	1.26	13.66 ± 0.06
$Na_{0.8}Fe_{0.8}Ti_{0.2}O_2$	1123 K, 3 h	3.76	92	1.4	20.5	33	1.73	16.0 ± 0.4
$Na_3Si_2Zr_{1.88}Y_{0.12}PO_{11.94}$ (NTZP20)	1503 K, 10 h	3.23	∼100	1.0	262	34	∼1	6.41 ± 0.04
$Na_{3.2}Si_{2.2}Zr_{1.88}Y_{0.12}P_{0.8}O_{11.94}$ (NTZP22)	1533 K, 8 h	3.22	99	3.0	99.1	34	1.70	5.89 ± 0.02

*ρ_{exp} corresponds to experimental ceramics density; ρ_{theor} corresponds to theoretical density of the compound calculated from crystal structure data.

**σ_{wet} corresponds to $p(H_2O) = 0.46$ atm. for the layered phases and to $p(H_2O) = 0.31$ atm. for NASICONs.

performed using a SETARAM TG-DTA LabSys instrument. The ionic transference numbers measurements by e.m.f. method were performed at room temperature using Na^+,Pt|$Na_{0.68}Ni_{0.34}Ti_{0.66}O_2$|Pt,$Na^+$ cells where the sodium activity at the electrodes was determined by $(CH_3COO)Na$ concentration in ethanol solutions.

3. Results and Discussion

3.1. Materials Characterization

For $Na_{0.68}Ni_{0.34}Ti_{0.66}O_2$ (P2-type), $Na_{0.8}Ni_{0.4}Ti_{0.6}O_2$ (O3) and mixed nickel-sodium antimonate $Na_{0.8}Ni_{0.6}Sb_{0.4}O_2$ (O3) synthesized for the first time, the use of the sintering conditions given in Table 1 made it possible to prepare single-phase ceramics with density higher than 91%. In the case of $Na_{0.8}Fe_{0.8}Ti_{0.2}O_2$ (O3), trace amounts of β-$NaFeO_2$ were detected by XRD. The formation of this phase cannot be suppressed increasing the sintering temperature; the processing conditions of $Na_{0.8}Fe_{0.8}Ti_{0.2}O_2$ were thus optimized in order to simultaneously obtain minimum secondary phase concentration (∼3%) and maximum density (∼92%). As a particular result, SEM micrographs of $Na_{0.8}Fe_{0.8}Ti_{0.2}O_2$ ceramics show small grains of irregular shape, while for other layered phases the grains have platelet shape characteristic of layered hexagonal structure (Fig. 1). The grain size of Ti-containing materials increases with sintering temperature. On the contrary, Sb-containing ceramics are characterized by a relatively small grain size and less glassy phase at the boundaries, although the sintering temperature in this case is quite high (Table 1).

As reported previously [19–21], using of TZP instead of monoclinic zirconia as a precursor for NASICON synthesis provides NASICON ceramics with a fine microstructure and minimum free ZrO_2 as impurity, usually found along the boundaries of this type of materials. In the present work, the highest densification was achieved for $Na_3Si_2Zr_{1.88}Y_{0.12}PO_{11.94}$ (NTZP20); $Na_{3.2}Si_{2.2}Zr_{1.88}Y_{0.12}P_{0.8}O_{11.94}$ (NTZP22) possesses a poor sinterability resulting in significant porosity (Fig. 1). Traces of monoclinic ZrO_2 were registered for both NASICON materials. Note that the presence of this zirconia impurity is due to Na and P losses by volatilization or by segregation as glassy phases at the grain boundaries, in both cases resulting from the relatively high sintering temperature, rather than to unreacted precursors [20–21].

Table 2 summarizes XRD data collection conditions and Rietveld refinement results; selected examples of the observed and calculated diffraction patterns are shown in Fig. 2. The structural data obtained for

Table 2. Structural properties, XRD data collection and Rietveld refinement details.

Composition	$Na_{0.68}Ni_{0.34}Ti_{0.66}O_2$	$Na_{0.8}Ni_{0.4}Ti_{0.6}O_2$	$Na_{0.8}Fe_{0.8}Ti_{0.2}O_2$	$Na_{0.8}Ni_{0.6}Sb_{0.4}O_2$	$Na_3Si_2Zr_{1.88}Y_{0.12}PO_{11.94}$	$Na_{3.2}Si_{2.2}Zr_{1.88}Y_{0.12}P_{0.8}O_{11.94}$
Structure type	P2	O3	O3	O3	NASICON	NASICON
Crystal system:	trigonal	trigonal	Trigonal	trigonal	monoclinic	monoclinic
Space group:	$P6_3/mmc$ (no. 166)	R-3 m (no. 166)	R-3 m (no. 166)	R-3 m (no. 166)	C 1 2/c 1 (no. 15)	C 1 2/c 1 (no. 15)
Unit cell dimensions (Å, degrees)	$a = 2.96226(8)$ $b = 11.1496(4)$	$a = 2.983(1)$ $b = 16.374(5)$	$A = 3.0019(1)$ $b = 16.3677(9)$	$a = 3.04820(7)$ $b = 16.3993(5)$	$a = 15.690(1)$ $b = 9.0782(7)$ $c = 9.2339(8)$ $\beta = 123.968(4)$	$a = 15.7418(7)$ $b = 9.1052(4)$ $c = 9.2108(4)$ $\beta = 124.223(2)$
Cell volume (Å^3)	84.73	126.18	127.75	131.97	1090.81	1091.62
Z (formula units per cell)	2	3	3	3	4	4
Theoretical density (g/cm^3)	3.887	4.059	4.089	5.078	3.232	3.253
2θ range (°)	10–130	10–130	10–130	10–130	10–90	10–90
Number of data points	6000	6000	6000	6000	8000	8000
Number of reflections	48	45	44	46	575	533
Number of parameters	21	20	19	19	59	59
Agreement factors						
R_p (%)	9.37	7.44	14.4	8.33	3.54	2.95
R_{wp} (%)	12.7	9.53	19.4	10.8	4.67	3.91
R_{exp} (%)	7.07	7.19	10.78	4.91	1.86	1.76
χ^2	3.21	1.76	3.25	4.81	6.28	4.92

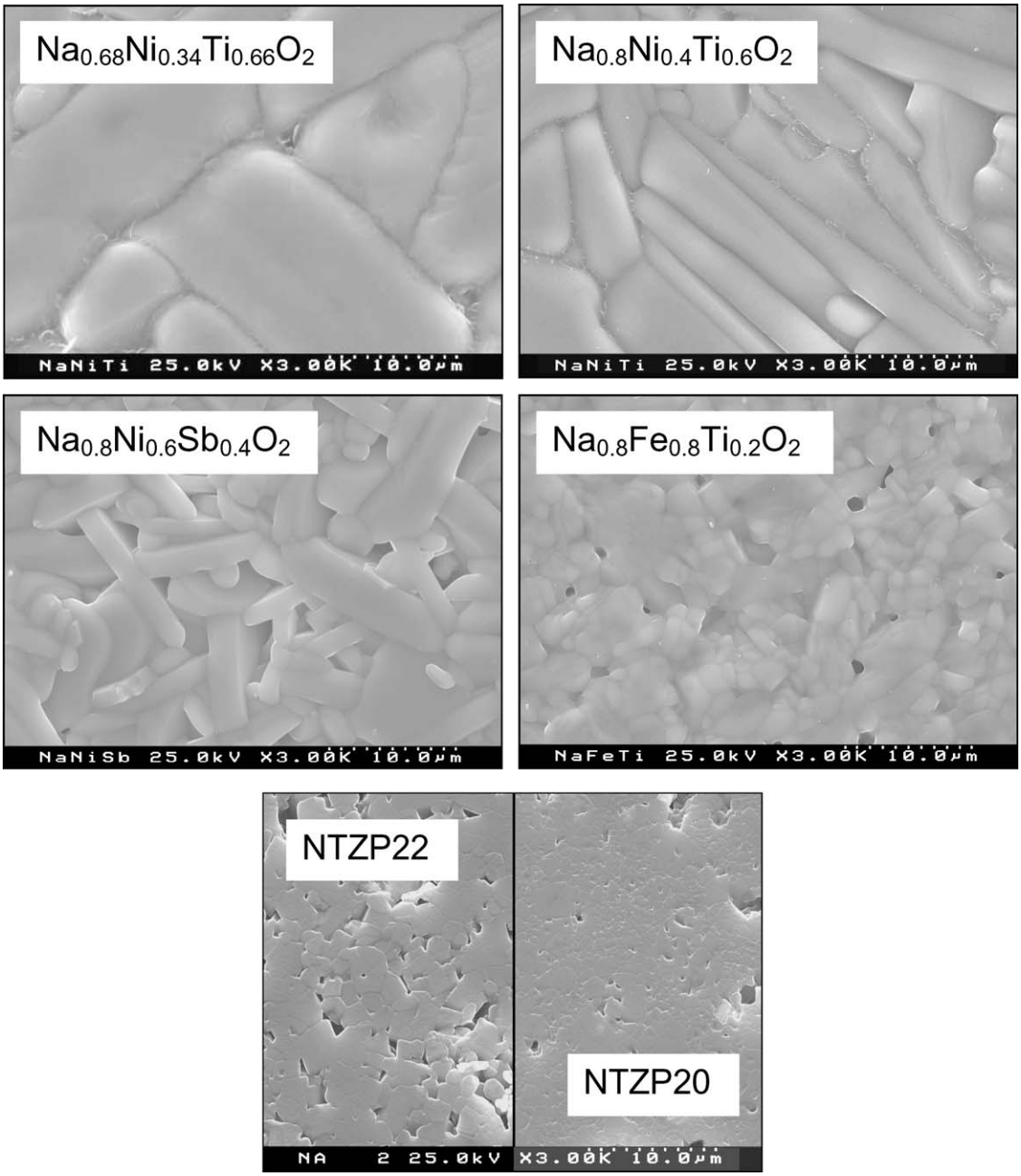

Fig. 1. SEM micrographs of Na^+-conducting ceramics.

nickel-sodium titanates $Na_{0.68}Ni_{0.34}Ti_{0.66}O_2$ (P2) and $Na_{0.8}Ni_{0.4}Ti_{0.6}O_2$ (O3) are in a good agreement with the literature [12]. The new mixed nickel-sodium antimonate, $Na_{0.8}Ni_{0.6}Sb_{0.4}O_2$, was found isostructural with $Na_{0.8}Ni_{0.4}Ti_{0.6}O_2$. In this structural family, the lattice parameter **a** is equal to the edge of MO_6 (M = Ni^{2+}, Fe^{3+}, Ti^{4+}, Sb^{5+}) octahedra. Increasing the average radius of M cations, randomly placed in octahedral sites, in the sequence $Na_{0.68}Ni_{0.34}Ti_{0.66}O_2$ (0.774 Å) > $Na_{0.8}Ni_{0.4}Ti_{0.6}O_2$ (0.779 Å) > $Na_{0.8}Ni_{0.6}Sb_{0.4}O_2$

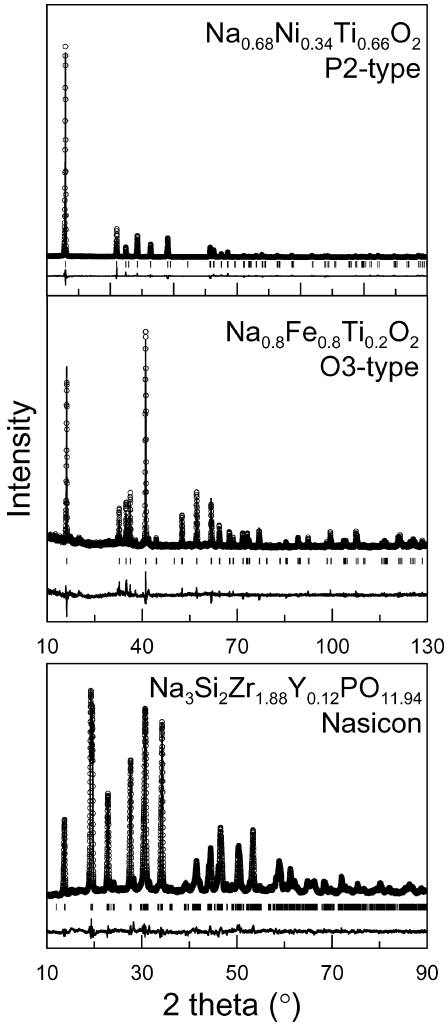

Fig. 2. Final observed, calculated and difference XRD patterns of the compounds with P2-, O3- and NASICON-type structure.

(0.794 Å) leads therefore to increasing **a** parameter. $Na_{0.8}Fe_{0.8}Ti_{0.2}O_2$ has a slightly lower average *M* radius (0.777 Å), but slightly larger **a** parameter as compared to $Na_{0.8}Ni_{0.4}Ti_{0.6}O_2$, due to the higher ionicity of (Fe, Ti)—O bonds. The parameter **c**, determined by the interlayer distance, depends on the amount of sodium ions sandwiched between $MO_{6/3}$ layers. Since decreasing sodium content results in a higher repulsion of oxygen anions, the interlayer distance in $Na_{0.68}Ni_{0.34}Ti_{0.66}O_2$ lattice is larger than that of other layered phases. $Na_3Si_2Zr_{1.88}Y_{0.12}PO_{11.94}$ and $Na_{3.2}Si_{2.2}Zr_{1.88}Y_{0.12}P_{0.8}O_{11.94}$ crystallize in the monoclinic symmetry with unit cell constants similar to $Na_3Si_2Zr_2PO_{12}$ [22].

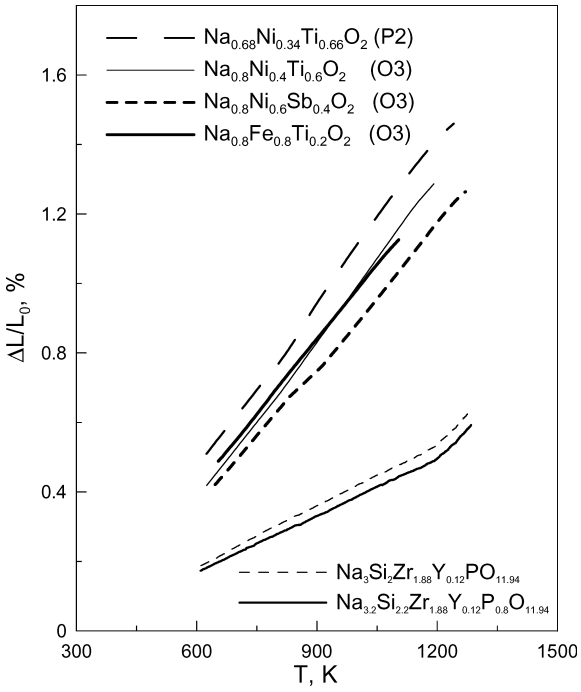

Fig. 3. Dilatometric curves of Na^+-conducting ceramics.

3.2. *Thermal Expansion*

Dilatometric studies of all studied materials showed that their thermal expansion at 300–1173 K can be described with a standard linear model (Fig. 3). The average thermal expansion coefficients (TECs) of Ni-containing compounds decrease from 15.7×10^{-6} to 13.7×10^{-6} K^{-1} when the concentration of nickel cations in the octahedral layers increase from 34 to 60%. The TEC value of $Na_{0.8}Fe_{0.8}Ti_{0.2}O_2$ is higher, 16.0×10^{-6} K^{-1}. These variations in thermal expansion coefficients, and also the absolute TEC values are quite similar to those of Ni- and Fe-containing perovskite oxides [23].

As for oxygen ion-conducting solid electrolytes [24], the isostructural O3-type compounds ($Na_{0.8}Ni_{0.6}Sb_{0.4}O_2$, $Na_{0.8}Fe_{0.8}Ti_{0.2}O_2$ and $Na_{0.8}Ni_{0.4}Ti_{0.6}O_2$) show a linear correlation between the conductivity and thermal expansion coefficients (Fig. 4). This behavior can be qualitatively explained in terms of the phenomenological theory of ionic transport [25] suggesting that the mobility of ionic defects increases with the thermal expansion of the crystal.

Thermal expansion of NASICON ceramics is considerably lower than that of phases with layered

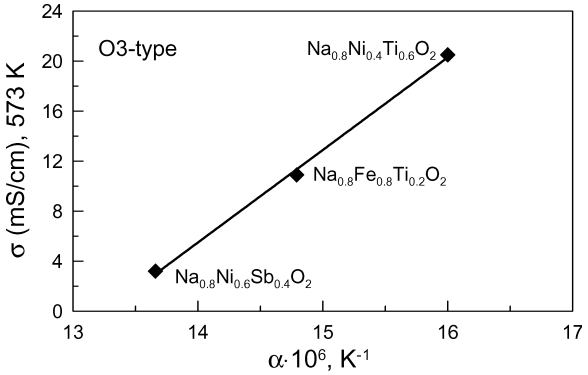

Fig. 4. Relationship between conductivity and thermal expansion coefficients of layered materials with the O3-type structure.

structure (Table 1). The TECs of NASICONs, (5.9–6.4) × 10^{-6} K^{-1}, are compatible with the expansion of commonly-used construction materials such as porcelain, which is advantageous for electrochemical applications. At temperatures above 1200 K, however, a significant change in the slope of dilatometric curves of Na^+ cation-conducting ceramics was observed (Fig. 3). Although additional studies are necessary to reveal the exact reasons for such phenomenon, one may suppose that such behavior is associated with formation of liquid phase. To our knowledge, a complete phase diagram for the quaternary Na_2O-ZrO_2-SiO_2-P_2O_5 system was not published; however, all numerous literature data on the Na_2O-SiO_2-P_2O_5 and Na_2O-SiO_2-ZrO_2 ternary systems point to the formation of liquid in the temperature range from 1123 to 1323 K, the lower limit corresponding to P_2O_5-rich compositional domain and the higher to the ZrO_2 one. Note that no phase transition is known to occur in NASICON at ca. 1200 K [26].

3.3. *Conductivity in Dry Atmospheres*

The temperature dependencies of total conductivity (σ) determined from the impedance spectra in dry atmospheres, are plotted in Fig. 5. On the contrary to transition metal-containing bronzes, the phases with brucite-like layers, including sodium-nickel titanates, are well known as solid electrolytes with negligible electron transference numbers [10, 27, 28]. In particular, one of the most probable origins of electronic conductivity, partial oxidation of Ni^{2+} to Ni^{3+}, is unfavorable due to mixing of Ni^{2+} with acidic Ti^{4+} or Sb^{5+} cations

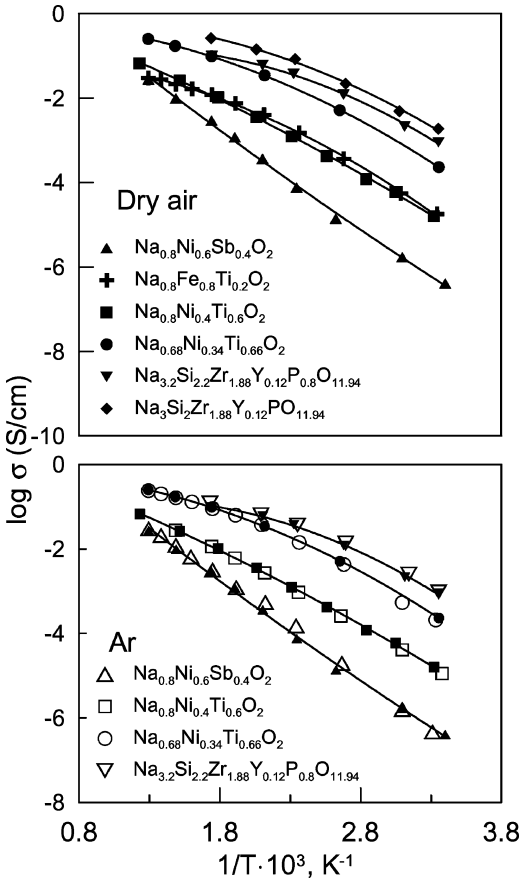

Fig. 5. Temperature dependence of total conductivity of the studied materials in dry air (top) and dry argon (bottom).

in the octahedral sites. Indeed, at temperatures below 700 K the ion transference numbers (t_{ion}), evaluated from e.m.f. of Na^+ concentration cells and using Hebb-Wagner technique, are higher than 0.99. One example is presented in Table 3 listing the values of t_{ion}, measured by the modified e.m.f. technique taking electrode polarization into account [29], for $Na_{0.68}Ni_{0.34}Ti_{0.66}O_2$ phase. Similar results were obtained for all studied

Table 3. Sodium cation transference numbers of $Na_{0.68}Ni_{0.34}Ti_{0.66}O_2$ determined by modified e.m.f. technique at 298 K using ethanol solutions with different Na^+ activities.

Na^+ concentration gradient	t_{ion}
0.1/0.01 M	0.9999
0.1/0.002 M	0.9996
0.1/0.0001 M	0.9996

materials; detailed data on their electronic conductivity will be published in a separate paper. As expected, the total conductivity of studied compounds is independent of the oxygen partial pressure, at least in the range from 0.21 atm. (dry air) to 1×10^{-5} atm (dry argon), Fig. 5. Therefore, the variations in σ values due to changes in the water vapor partial pressure, discussed below, cannot be attributed to variations in the electronic transport from oxygen loss or incorporation into the lattice. In general, when analyzing trends and the σ vs. $p(H_2O)$ dependence, the electronic transport in the studied Na^+-conducting ceramics can be neglected.

The sodium cationic conductivity increases in the series O3-type < P2 < NASICON (Fig. 5). This trend can be mainly explained by structural effects with relevance on the cation diffusion pathway. The NASICON structure has a three-dimensional network formed by channels available for ionic transport, whilst in the layered compounds the conduction is two-dimensional. Among layered phases, the structures with prismatic coordination of sodium show typically a higher conductivity with respect to octahedral [10, 12]. For P2-type structure, Na^+ ions are distributed within a layer of equivalent prisms forming wide square bottlenecks. This leads to a considerably higher mobility than that in O3-type lattice comprising octahedral sodium hosts, small tetrahedrally-coordinated interstitial positions and triangle bottlenecks between them. For O3-type phases, the conductivity of $Na_{0.8}Ni_{0.4}Ti_{0.6}O_2$ and $Na_{0.8}Fe_{0.8}Ti_{0.2}O_2$ is higher than that of $Na_{0.8}Ni_{0.6}Sb_{0.4}O_2$ presumably due to shorter jump distances between sodium sites, which may be expressed by the **a** parameter (Table 2).

Another necessary comment relates to an important role of ceramic microstructure. In particular, the conductivity of the layered titanates (Fig. 5) is substantially higher than the values reported for similar ceramic materials, $Na_{0.8}Fe_{0.8}Ti_{0.2}O_2$ [11] and $Na_xNi_{x/2}Ti_{1-x/2}O_2$ [10, 12,13]. Most likely, this is a result of higher density achieved in this work. On the contrary, NTZP22 ceramics has a lower conductivity than NTZP20 due to a poor microstructure, as mentioned above.

3.4. *Water Absorption and Conductivity in H_2O-Containing Atmospheres*

At high temperatures the conductivity of all studied materials was found essentially independent of air humidity. At temperatures around 323 K, however, the presence of water vapor in the atmosphere results in apparent higher σ values, as illustrated by Fig. 6. The observed changes are completely reversible—the initial values of the impedance can be reproduced after experiments with an accuracy of 3–5%, comparable to the conductivity measurement error (Fig. 7). In order to assess possible mechanisms of interaction with water, a series of ceramic samples were hydrated in wet air at 373 K and $p(H_2O) = 0.46$ atm. for 24 h, ground into powders and then studied by XRD and TG/DTA. The time necessary to achieve equilibrium water content

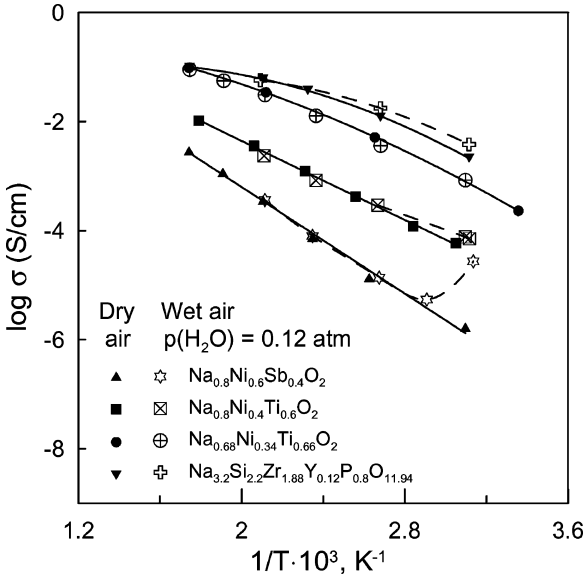

Fig. 6. Temperature dependence of total conductivity of the studied materials in wet air.

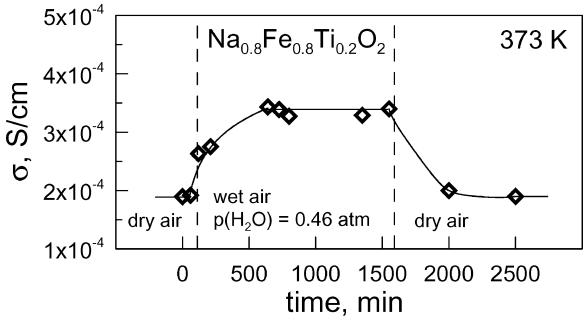

Fig. 7. Time dependence of conductivity of $Na_{0.8}Fe_{0.8}Ti_{0.2}O_2$ ceramics after $p(H_2O)$ variations, showing reversibility and approximate relaxation time.

was estimated from the conductivity relaxation data (Fig. 7).

As mentioned above, the layered phases can absorb water between $MO_{6/3}$ layers sandwiching sodium cations. One may hence expect an increase in the interlayer distance and, thus, lattice parameter **c** due to water incorporation. Indeed, for $Na_{0.8}Ni_{0.4}Ti_{0.6}O_2$ and $Na_{0.8}Ni_{0.6}Sb_{0.4}O_2$ samples kept in wet air, XRD shows an appearance of second hydrated phase having larger **c** and essentially unchanged **a** parameters. In Fig. 8(a) and (c) the reflections of hydrated phases are marked with subscript "aq"; as expected, the (003) and (006) reflections are strongly shifted towards lower 2θ angles. The **c** parameter calculated from 7–10 reflections with high l-contribution (003, 006, 009, 018 etc.), increased by approximately 30% and is equal to 21.50 and 21.38 Å for hydrated $Na_{0.8}Ni_{0.4}Ti_{0.6}O_2$ and $Na_{0.8}Ni_{0.6}Sb_{0.4}O_2$, respectively; the **a** parameter is 3.00 Å for both hydrated phases. One should also note that the amount of hydrated phase formed in $Na_{0.8}Ni_{0.4}Ti_{0.6}O_2$ ceramics is substantially larger than that in $Na_{0.8}Ni_{0.6}Sb_{0.4}O_2$.

No evidence for the intercalation of water in to the interlayer space was observed in the XRD patterns of P2-type $Na_{0.68}Ni_{0.34}Ti_{0.66}O_2$ and O3-type $Na_{0.8}Fe_{0.8}Ti_{0.2}O_2$ (Fig. 8(e) and (f)) after treatment with water vapor. In the latter case, however, the XRD pattern shows a significant amount of $Na_2CO_3{\cdot}H_2O$, marked in Fig. 8(g) by filled circles. Such a behavior could be ascribed either to increasing sodium deficiency or to a partial ionic exchange followed by the reaction with atmospheric CO_2, for example:

$$Na_{0.8}Fe_{0.8}Ti_{0.2}O_2 + (0.8x)H_2O + (0.4x)CO_2 \rightarrow (Na_{1-x}H_x)_{0.8}Fe_{0.8}Ti_{0.2}O_2 + (0.4x)Na_2CO_3{\cdot}H_2O$$

The fact, that the unit cell parameters are essentially unaffected by interaction with water, suggests that this reaction primarily occurs in $Na_{0.8}Fe_{0.8}Ti_{0.2}O_2$ surface layers and/or at the grain boundaries. Moderate amounts of $Na_2CO_3{\cdot}H_2O$ were also observed in the XRD patterns of $Na_{0.8}Ni_{0.4}Ti_{0.6}O_2$ (Fig. 8(a)), while $Na_{0.8}Ni_{0.6}Sb_{0.4}O_2$ and $Na_{0.68}Ni_{0.34}Ti_{0.66}O_2$ contain only trace amounts of this phase; in the latter case the peaks are almost coincident with the pattern background and thus unmarked in Fig. 8(e).

As it reported previously [30], interaction of NASICON-type phases with liquid water leads to the formation of the H_3O^+-substituted compound, the so-

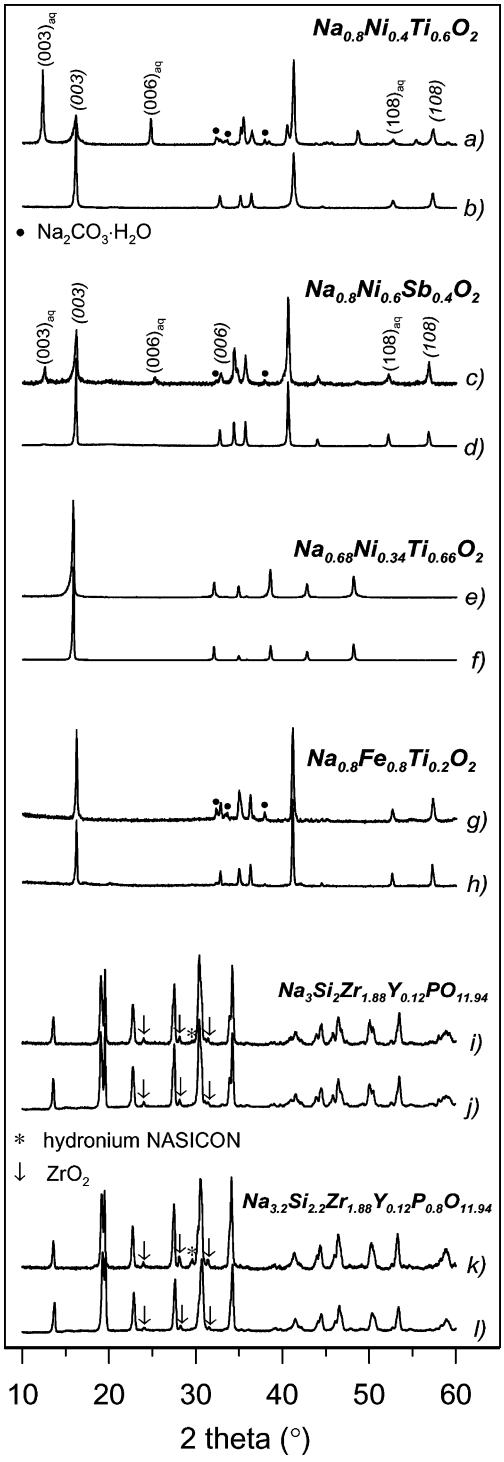

Fig. 8. Comparison of the XRD patterns of studied materials after hydration (a, c, e, g, i, k) and after annealing (b, d, f, h, j, l). Hydrated ceramics were kept in wet air at 373 K and $p(H_2O) = 0.46$ atm. for 24 h. Subsript "aq" shows peaks of hydrated layered phases.

called hydronium NASICON. Results of the present work show that treatment with water vapor has the same effect, the highest intensity peaks of the hydration/ion exchange product are marked with asterisks in Fig. 8(i) and (k). In the case of NTZP20 ceramics, the amount of hydronium NASICON is negligible and can hardly be recognized in the scale used in Fig. 8(i). The lower stability of NTZP22 ceramics may be partly explained by the porous microstructure and thus considerably larger area exposed to the moisture atmosphere, but probably also due to the higher sodium content.

TG/DTA showed that heating of all hydrated materials up to 330–380 K results in a substantial weight loss, which is accompanied by endothermal DTA effects and can be undoubtedly attributed to water evaporation (Fig. 9). Notice that dehydration of $Na_2CO_3 \cdot H_2O$ may be expected at 370–420 K, whilst decomposition of Na_2CO_3 occurs at considerably higher temperatures [31]. For the layered compounds, the water content per one sodium ion, extracted from thermogravimetric data, increases in a sequence $Na_{0.8}Ni_{0.4}Ti_{0.6}O_2 < Na_{0.8}Ni_{0.6}Sb_{0.4}O_2 < Na_{0.68}Ni_{0.34}Ti_{0.66}O_2 < Na_{0.8}Fe_{0.8}Ti_{0.2}O_2$. This seems on the contrary to XRD results, suggesting maximum stability for $Na_{0.68}Ni_{0.34}Ti_{0.66}O_2$ and, possibly, $Na_{0.8}Ni_{0.6}Sb_{0.4}O_2$ phases. One can hence assume that water absorption in $Na_{0.68}Ni_{0.34}Ti_{0.66}O_2$ and $Na_{0.8}Ni_{0.6}Sb_{0.4}O_2$ occurs, to a considerable extent, via interaction with glassy phases and/or formation of amorphous hydrates at the grain boundaries, which cannot be detected by XRD.

Typical impedance spectra obtained at different temperatures and water vapor partial pressures are shown in Figs. 10 and 11. For $Na_{0.68}Ni_{0.34}Ti_{0.66}O_2$ and $Na_{0.8}Ni_{0.4}Ti_{0.6}O_2$, a single depressed semicircle is observed. The existence of two contributions, although overlapping to some degree, is apparent for $Na_{0.8}Ni_{0.6}Sb_{0.4}O_2$ and is clearly observed for the two NASICONs and $Na_{0.8}Fe_{0.8}Ti_{0.2}O_2$. The high and low frequency semicircles may be ascribed to grain and grain boundary impedances, respectively. A tentative fit to the equivalent circuit consisting of a series of two elements comprising a resistor in parallel with a capacitor is shown for $Na_{0.8}Ni_{0.6}Sb_{0.4}O_2$ in Fig. 11. The trend observed for $Na_{0.8}Fe_{0.8}Ti_{0.2}O_2$ is very similar. Although the quality of the fit is, in some cases, insufficient, it seems that the grain boundary is more affected by humidity than the bulk, at least at temperatures below 373 K when maximum water absorption is observed. This effect may be determined by numerous factors, including sodium content, porosity,

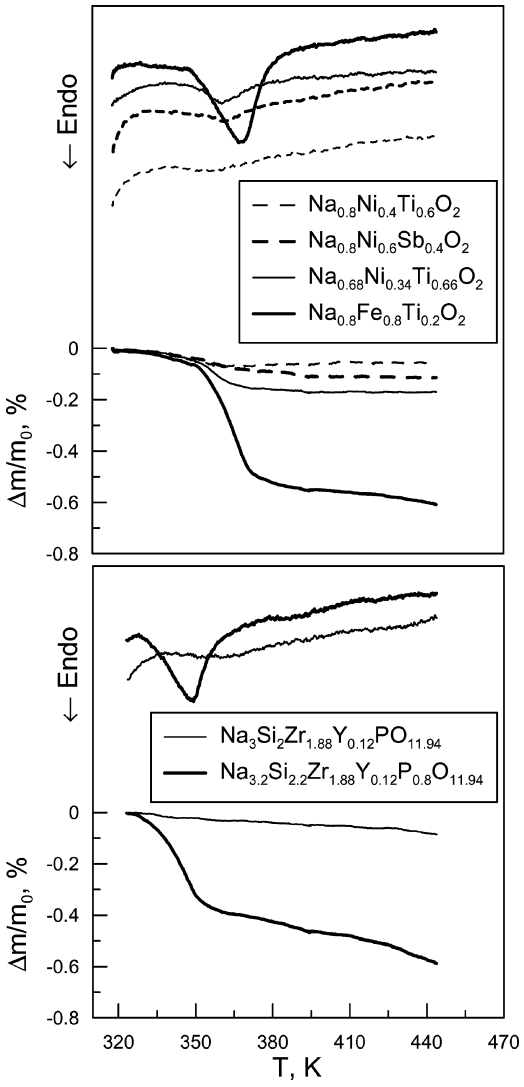

Fig. 9. TG and DTA curves of ceramic materials after hydration. Ceramics were kept in wet air at 373 K and $p(H_2O) = 0.46$ atm. for 24 h, and then ground into powders.

grain-boundary area, or the presence of glassy phases at the grain boundaries. Since the stronger effect is observed at temperatures lower 373 K, water condensation in the pores or over the sample and platinum electrodes should not be excluded. This may be illustrated by the example of NASICON ceramics. The total conductivity of NTZP20 is essentially independent on air humidity, whilst NTZP22 shows a 70% increase of the conductivity in humid air (Table 1). Such an effect correlates with higher Na^+ content in NTZP22, porous microstructure of NTZP22 ceramics (Fig. 1)

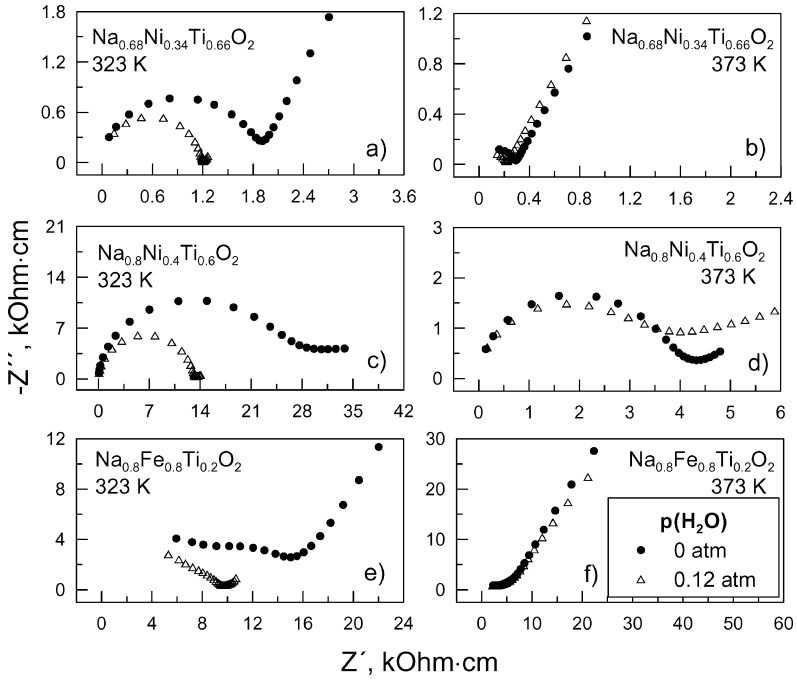

Fig. 10. Typical impedance spectra of Na^+-conducting ceramics in dry and wet air. In all cases, water vapor partial pressure in wet air is 0.12 atm.

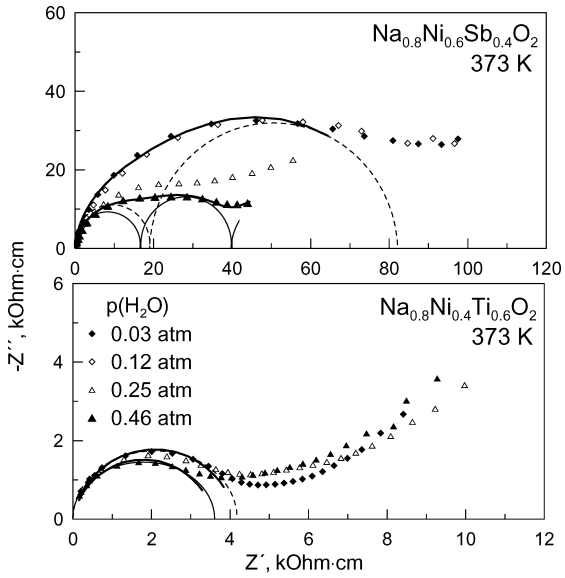

Fig. 11. Impedance spectra in atmospheres with various $p(H_2O)$. Thick solid lines show fitting results of high-frequency parts of the spectra using the simplest adequate models. Dashed and thin solid semicircles indicate elements of equivalent circuit built from resistance and capacitance connected in parallel and correspond to wet atmospheres with $p(H_2O) = 0.03$ atm. and $p(H_2O) = 0.46$ atm., respectively.

and water content extracted from TG-DTA data (Fig. 9). Then, for layered materials, the sensitivity of total conductivity to air humidity increases in the sequence $Na_{0.8}Ni_{0.4}Ti_{0.6}O_2 < Na_{0.68}Ni_{0.34}Ti_{0.66}O_2 < Na_{0.8}Ni_{0.6}Sb_{0.4}O_2 < Na_{0.8}Fe_{0.8}Ti_{0.2}O_2$ (Table 1), which correlates well with the increasing grain-boundary area of the ceramics except for $Na_{0.68}Ni_{0.34}Ti_{0.66}O_2$ which possesses much larger grains than in $Na_{0.8}Ni_{0.4}Ti_{0.6}O_2$ but exhibit a slightly higher conductivity increase. The latter can be explained by a higher amount of glassy phases at the grain boundaries in $Na_{0.68}Ni_{0.34}Ti_{0.66}O_2$ (Fig. 1) due to a high sintering temperature, close to melting point. Finally, the maximum stability in wet atmospheres was found for $Na_3Si_2Zr_{1.88}Y_{0.12}PO_{11.94}$, while the other NASICON-type phase $Na_{3.2}Si_{2.2}Zr_{1.88}Y_{0.12}P_{0.8}O_{11.94}$ and the layered $Na_{0.8}Fe_{0.8}Ti_{0.2}O_2$ material are unstable.

4. Conclusions

Sodium cation-conducting ceramics of layered phases $Na_{0.68}Ni_{0.34}Ti_{0.66}O_2$ (P2-type structure), $Na_{0.8}Ni_{0.4}Ti_{0.6}O_2$, $Na_{0.8}Fe_{0.8}Ti_{0.2}O_2$, $Na_{0.8}Ni_{0.6}Sb_{0.4}O_2$ (O3-type structures) and NASICON-type $Na_3Si_2Zr_{1.88}Y_{0.12}PO_{11.94}$ and $Na_{3.2}Si_{2.2}Zr_{1.88}Y_{0.12}P_{0.8}O_{11.94}$ were

prepared by the standard solid-state reaction technique. The dilatometric studies showed that thermal expansion of Na^+-conducting ceramics is linear at 300–1173 K, with average TEC values varying in the range (13.7–16.0) $\times$ 10^{-6} K^{-1} for the layered materials and (5.9–6.5) $\times$ 10^{-6} K^{-1} for NASICON-type ceramics. The conductivity of O3-type compounds, predominantly ionic, shows a linear correlation with TECs. At 298–423 K, increasing vapor partial pressure from approximately 0 (dry air) to 0.46 atm. leads to water absorption, accompanied with increasing total conductivity of the studied materials, which is favored by higher sodium content. Analysis of the impedance spectra suggests that the increase in the conductivity has a dominantly grain-boundary nature. Due to the dominant role of boundaries, the interaction of studied materials with water vapor is strongly influenced by the ceramic microstructure. For layered materials, the sensitivity to partial water vapor pressure increases with decreasing grain size in the sequence $Na_{0.8}Ni_{0.4}Ti_{0.6}O_2$ < $Na_{0.8}Ni_{0.6}Sb_{0.4}O_2$ < $Na_{0.8}Fe_{0.8}Ti_{0.2}O_2$. Maximum stability in wet atmospheres was found for $Na_3Si_2Zr_{1.88}Y_{0.12}PO_{11.94}$ ceramics, which also exhibit the highest ionic conduction.

Acknowledgments

This work was supported by the FCT, Portugal (POCTI program and project BD/6594/2001) and ICDD (grant 00-15). Helpful discussions with V.B. Nalbandyan and J.R. Frade are gratefully acknowledged.

References

1. J.M. Paulsen, D. Larcher, and J.R. Dahn, *J. Electrochem. Soc.*, **147**, 2862 (2000).
2. V. Leonhard, H. Erdmann, M. Ilgenstein, K. Cammann, and J. Krause, *Sensors and Actuators B*, **18/19**, 329 (1994).
3. H. Khireddine, P. Fabry, A. Caneiro, and B. Bochu, *Sensors and Actuators B*, **40**, 223 (1997).
4. H. Yagi and T. Saiki, *Sensors and Actuators B*, **5**, 135 (1991).
5. T. Maruyama, S. Sasaky, and Y. Saito, *Solid State Ionics*, **23**, 107 (1987).
6. T. Kida, Y. Miyachi, K. Shimanoe, and N. Yamazoe, *Sensors and Actuators B*, **80**, 28 (2001).
7. H. Kohler and H. Schulz, *Mater. Res. Bull.*, **20**, 1461 (1985).
8. C.R. Peters, M. Bettman, J.W. Moore, and M.D. Glick, *Acta Cryst. B*, **24**, 1968 (1982).
9. A. Maazaz, C. Delmas, C. Fouassier, J.-M. Reau, and P. Hagenmuller, *Mater. Res. Bull.*, **14**, 193 (1979).
10. V.B. Nalbandyan and I.L. Shukaev, *Rus. J. Inorg. Chem.*, **37**, 1231 (1992).
11. E.I. Burmakin and G.Sh. Shekhtman, *Electrokhimiya*, **21**, 752 (1985) (in Russian).
12. Y.-L. Shin and M.-Y. Yi, *Solid State Ionics*, **132**, 131 (2000).
13. Y.-L. Shin, M.-H. Park, J.-H. Kwak, H. Namgoong, and O.H. Han, *Solid State Ionics*, **150**, 363 (2002).
14. Zh. Lu and J.R. Dahn, *Chem. Mater.*, **13**, 1252 (2001).
15. A. Ahmad, T.A. Wheat, A.K. Kuriakose, J.D. Canaday, and A.G. McDonald, *Solid State Ionics*, **24**, 89 (1987).
16. F. Mauvy, E. Siebert, and P. Fabry, *Talanta*, **48**, 293 (1999).
17. T. Kida, K. Shimanoe, N. Miura, and N. Yamazoe, *Sensors and Actuators B*, **75**, 179 (2001).
18. J. Rodrigues-Carvajal, *Physica B*, **192**, 55 (1993).
19. R.O. Fuentes, F.M.B. Marques, and J.I. Franco, *Bol. Soc. Esp. Ceram. Vidrio*, **38**, 631 (1999).
20. R.O. Fuentes, F.M. Figueiredo, F.M.B. Marques, and J.I. Franco, *J. Europ. Ceram. Soc.*, **21**, 737 (2001).
21. R.O. Fuentes, F.M. Figueiredo, F.M.B. Marques, and J.I. Franco, *Solid State Ionics*, **140**, 173 (2001).
22. W.H. Baur, J.R. Dygas, D.H. Whitmore, and J. Faber, *Solid State Ionics*, **18/19**, 935 (1986).
23. V.V. Kharton, A.A. Yaremchenko, and E.N. Naumovich, *J. Solid State Electrochem.*, **3**, 303 (1999).
24. V.V. Kharton, E.N. Naumovich, A.A. Yaremchenko, and F.M.B. Marques, *J. Solid State Electrochem.*, **5**, 160 (2001).
25. V.N. Chebotin, *Physical Chemistry of Solids* (Khimiya, Moscow, 1982) (in Russian).
26. P. Colomban, *Solid State Ionics*, **21**, 97 (1986).
27. C. Delmas, C. Fouassier, J.-M. Reau, and P. Hagenmuller, *Mater. Res. Bull.*, **11**, 1081 (1976).
28. M.Y. Avdeev, V.B. Nalbandyan, and B.S. Medvedev, *Inorg. Mater.*, **33**, 500 (1997).
29. A.A. Yaremchenko, V.V. Kharton, E.N. Naumovich, and F.M.B. Marques, *J Electroceramics*, **4**, 235 (2000).
30. R.O. Fuentes, F.M. Figueiredo, F.M.B. Marques, and J.I. Franco, *Solid State Ionics*, **139**, 309 (2001).
31. Phase Equilibria Diagrams, *CD-Rom Database*, edited by P. Schenck (The American Ceramic Society, Westerville, OH, 1998).